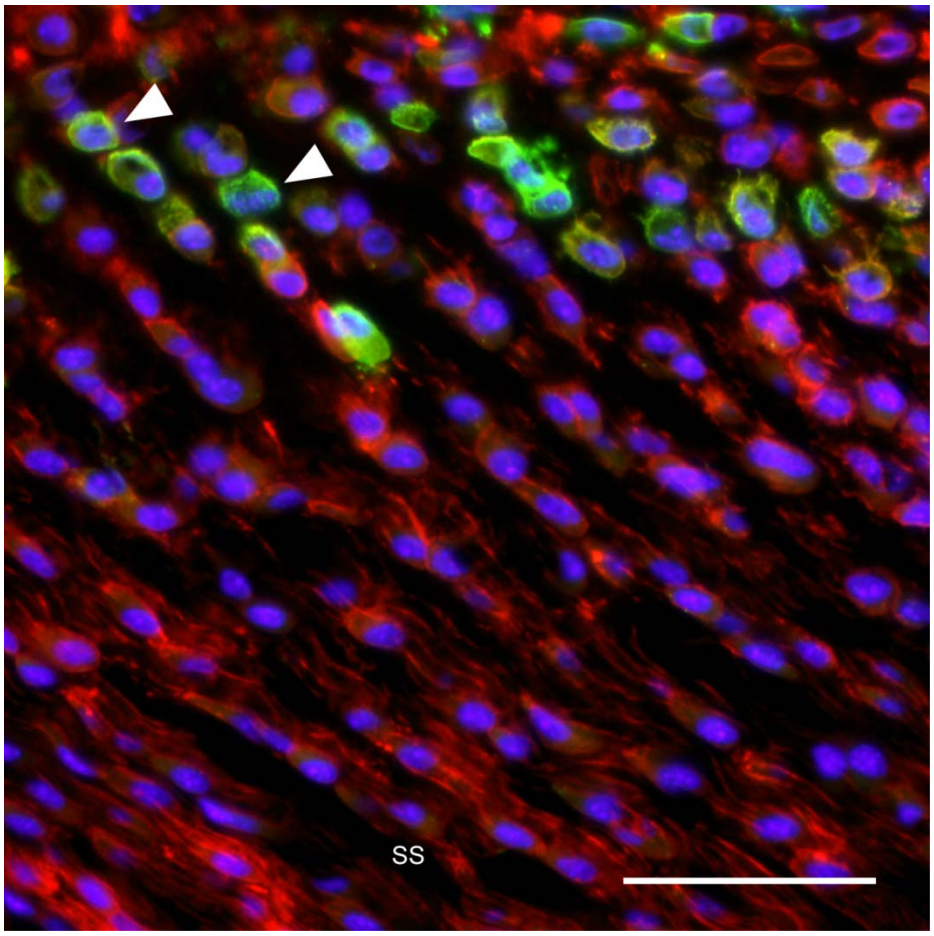

Figure S1: Gli1-positive cells (green) indicated by the arrowheads from a P7 Gli1Cre^{ERT2};mTmG mouse displayed a rounded cell morphology. Blue: DAPI nuclear stain. Scale = 50 μm.

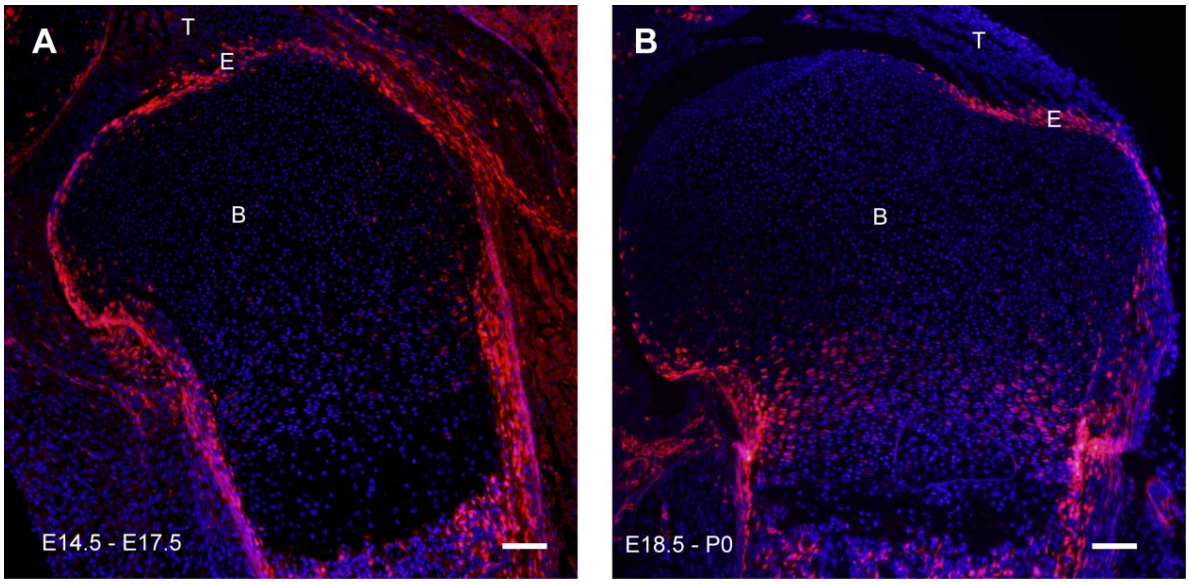

Figure S2: Gli1-positive cells (red) were visualized in the developing humerus. **(A)** Gli1Cre^{ERT2};Ai14 mouse labeled with TAM on E14.5 and euthanized on E17.5 exhibited Gli1-positive cells in the enthesis (E), perichondrium, and growth plate. **(B)** At E18.5, Gli1 expression was absent from the developing articular surface but remained in the enthesis and bone collar. Blue: DAPI nuclear stain. Scale = 100 μm. T: supraspinatus tendon, B: bone.

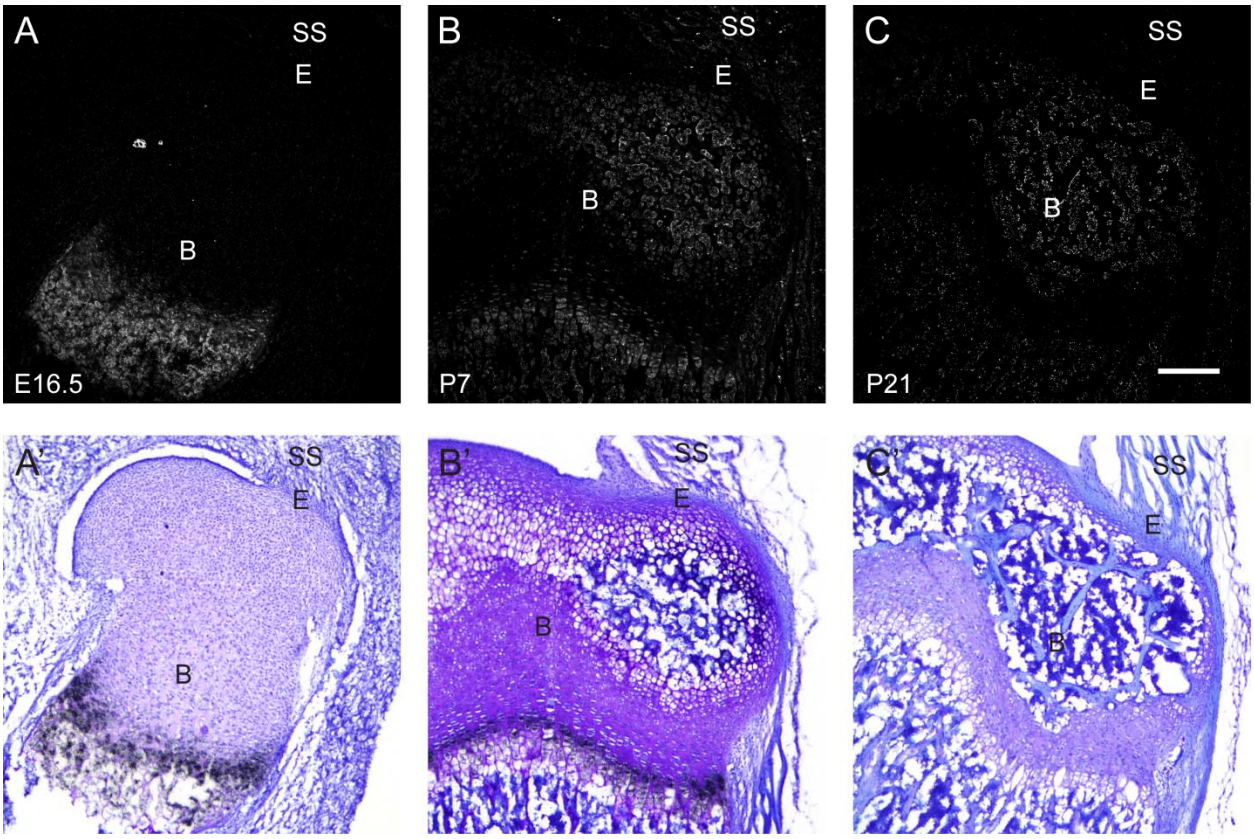

Figure S3: *In situ* hybridization for Ihh. Top panels: dark field, bottom panels: bright field counterstained with toluidine blue. **(A)** The source of the Ihh ligand at E16.5 was the primary ossification center of the humerus. **(B)** At P7, Ihh was found in the primary growth plate and in the secondary ossification center. **(C)** At P21, expression levels of Ihh decreased and were localized to the secondary ossification center. SS: Supraspinatus tendon, E: enthesis, B: bone Scale = 200 μm.

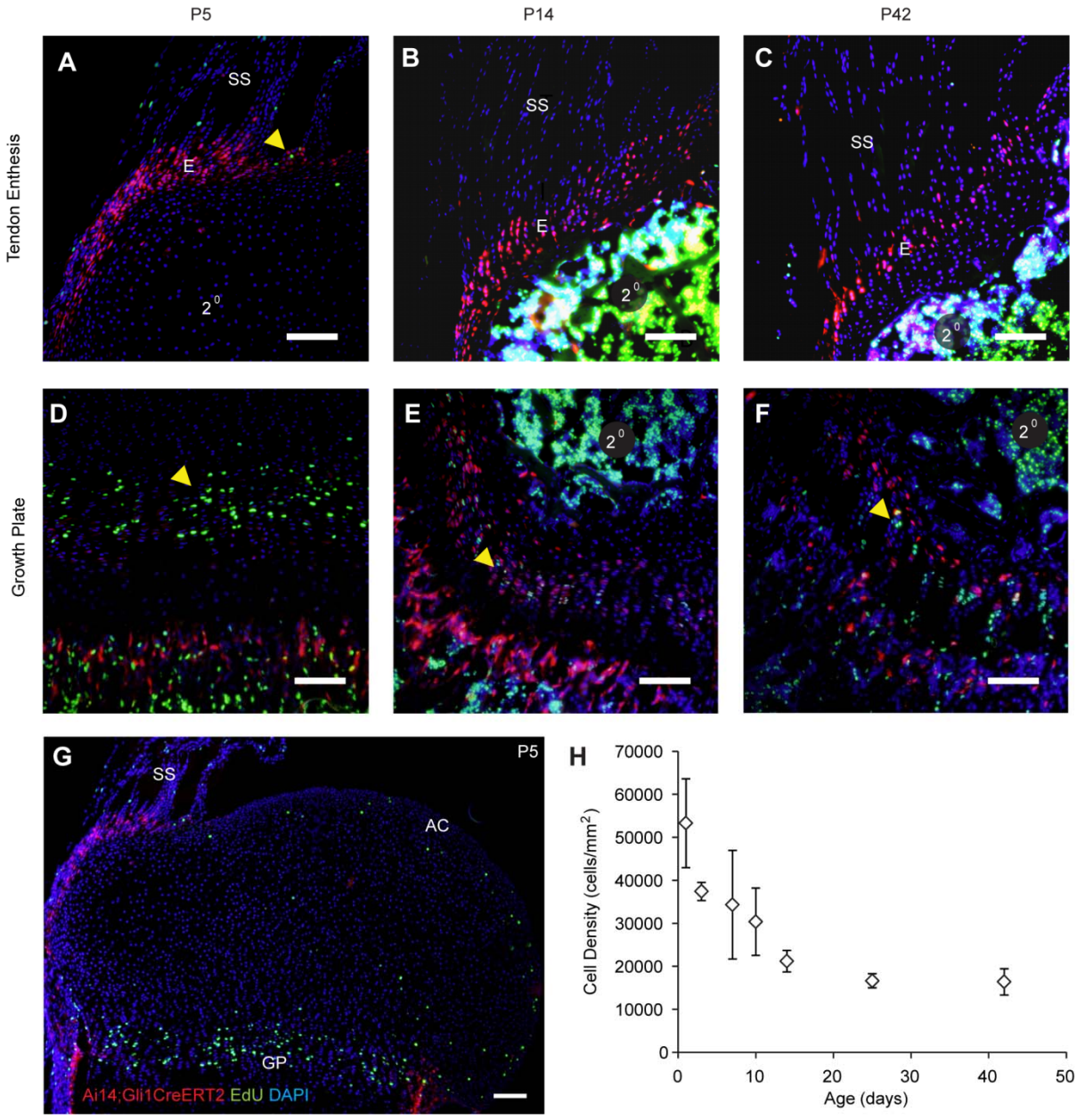

Figure S4: The Hh-responsive cell population at the enthesis does not proliferate rapidly. Cells from the supraspinatus (SS) enthesis (E) **(A-C)** and growth plate (GP) **(D-F)** were activated with TAM (red fluorescence) 2 days prior to sacrifice and EdU (green fluorescence) 2-4 hours prior to sacrifice on P5 (A, D), P14 (B, E), and P42 (C, F). The yellow arrow in (A) points to a few EdU positive cells in the P5 enthesis. The yellow arrows in (D-F) indicate proliferating (EdU positive) cells in the growth plate. **(G)** More EdU positive proliferating cells were observed in the growth plate, articular cartilage (AC), and supraspinatus tendon midsubstance (SS) than the Hh-responsive cell population within the tendon enthesis. **(H)** Cell density at the enthesis decreased as a function of animal age. 2^0: secondary ossification center of the humeral head. Scale bars = 100 μm.

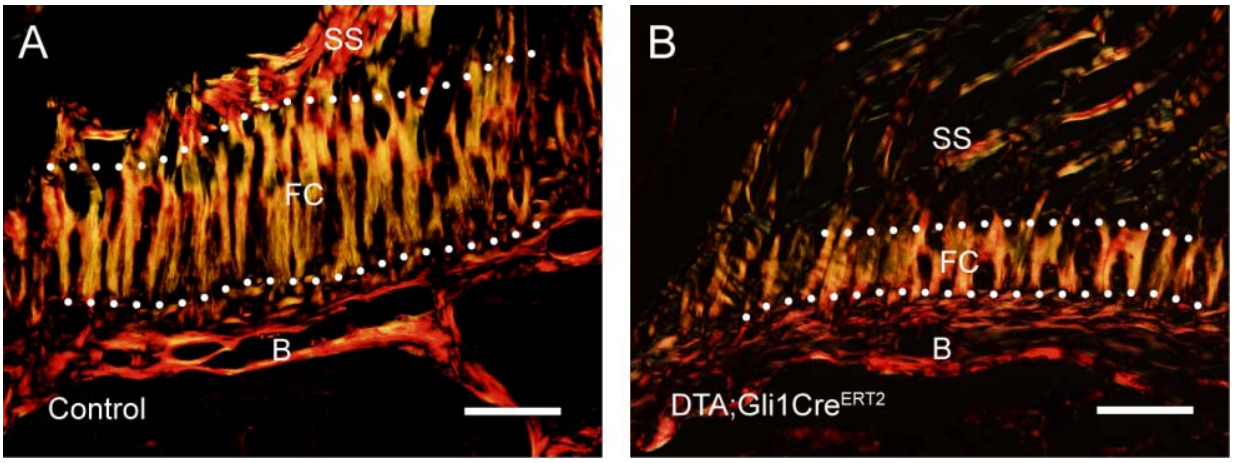

Figure S5: Picrosirius red stained supraspinatus tendon entheses from P42 **(A)** Control and **(B)** DTA;Gli1Cre^{ERT2} mice. The fibrocartilage thickness (between the dotted lines) is reduced in the ablated animals although the pattern of fiber alignment is consistent with controls. Scale = 100 μm.

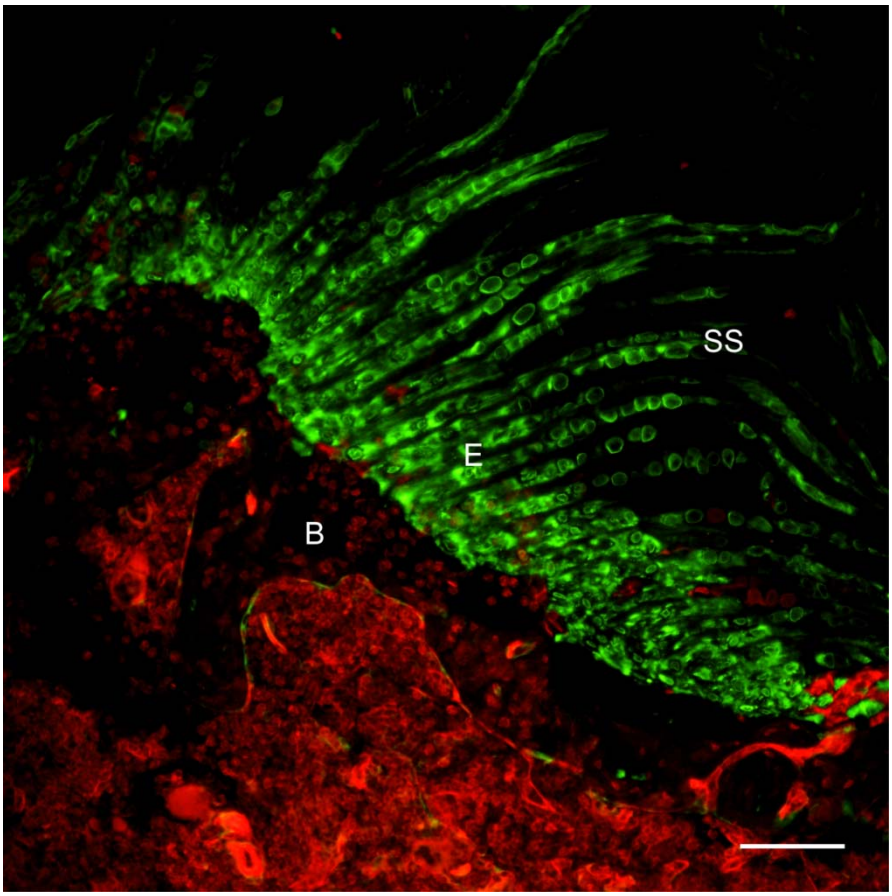

Figure S6: Supraspinatus tendon enthesis from a P56 ScxCre;mTmG mouse. The expression pattern of the ScxCre construct (green fluorescence) demonstrated targeting of cells from the enthesis fibrocartilage (E) as well as the tendon (SS), but not the underlying bone (B). Scale = 100 μm.

Supplementary Methods

X-ray diffraction and fluorescence mapping

X-ray fluorescence (XRF) and diffraction (XRD) experiments were performed at the Argonne National Lab using beamline 2I-D-D. Fresh frozen tendon insertions from ScxCre;Smo$^{fl/fl}$ animals and littermate controls (N=3 per group) were isolated, embedded in optimal cutting temperature (OCT) embedding medium, frozen at -80 °C, and sectioned at 20 μm on a cryostat. Frozen tissue sections were mounted on silicon nitride windows (Silson Ltd., Northampton, Eng.). Immediately prior to analysis, samples were defrosted and air dried. The OCT was not removed in order to minimize section adhesion to the silicon nitride windows and it was not detectable in the wide-angle X-ray scattering (WAXS) diffraction patterns. The silicon nitride mounted samples were attached to the sample holder using adhesive and placed normal to the incident X-ray beam at the focal plane of the X-ray zone plate. The enthesis was identified by preliminary optical mapping followed by X-ray fluorescence mapping of regions of MFC near the bone-tendon interface using a 250 nm x 250 nm X-ray beam. The XRF signal was collected with a Vortex-EX silicon drift detector (SII Nanotechnology USA, Northridge, CA) positioned as close to the specimen as possible and aligned to collect X-rays emerging nearly parallel to the front surface of the specimen and in the horizontal plane (i.e., the plane of the storage ring) for the best signal-to-noise ratio. Following preliminary mapping, 20 spots were analyzed within the fully mineralized MFC region arranged in 2 rows of 10 parallel to the mineral interface and spaced by 1 μm. XRF measurements at each spot were followed by collection of WAXS diffraction peaks from the mineral using a MAR165 CCD detector (Rayonix, Evanston, IL) placed behind the specimen. The acquisition time for each diffraction measurement was approximately 2 minutes. The acquired diffraction patterns for each region of interest were analyzed using custom software previously developed by Dr. Jon Almer (APS, Sector 1) and modified by Dr. Alix Deymier-Black for this application (Deymier-Black et al., 2013). The diffraction rings were fitted and measures of crystallite size, angular intensity, crystal strain, and root mean square strain (ε_{RMS}) were averaged over the 20 mapped spots for each specimen. Angular intensity was determined by fitting the peak intensity of the HAP(002) ring as a function of azimuthal angle calculating the FWHM. A wider distribution indicates less alignment of the mineral crystals. Crystal lattice strain was determined from the deviation from circularity of the HAP(002), HAP(211) and HAP(004) diffraction rings (Almer and Stock, 2007). Crystallite size and ε_{RMS} were calculated from the analysis of peak broadening as described previously (Deymier-Black et al., 2013). Briefly, instrumental broadening was removed by comparison to a ceria standard and the intensity of the HAP(002) and HAP(004) peaks were fitted using a pseudo-Voigt function. A modified version of Scherrer's equation was used to convert the experimentally determined peak widths into estimates of crystal size and ε_{RMS}. The ε_{RMS} is a measure of the variation of strains within the analysis volume.

Supplementary References

Almer, J. D. and Stock, S. R. (2007) 'Micromechanical response of mineral and collagen phases in bone', *J Struct Biol* 157(2): 365-70.

Deymier-Black, A. C., Singhal, A., Yuan, F., Almer, J. D., Brinson, L. C. and Dunand, D. C. (2013) 'Effect of high-energy X-ray irradiation on creep mechanisms in bone and dentin', *Journal of the mechanical behavior of biomedical materials* 21: 17-31.